ORIGINAL ARTICLE

3D Freeform Printing of Nanocomposite Hydrogels through *in situ* Precipitation in Reactive Viscous Fluid

Shengyang Chen[1], Tae-Sik Jang[2], Houwen Matthew Pan[1], Hyun-Do Jung[2], Ming Wei Sia[1], Shuying Xie[1], Yao Hang[3], Seow Khoon Mark Chong[1], Dongan Wang[4], Juha Song[1]*

[1]School of Chemical and Biomedical Engineering, Nanyang Technological University, 70 Nanyang Drive, 637457, Singapore

[2]Liquid Processing and Casting Technology R&D Group, Korea Institute of Industrial Technology, Incheon 406-840, Republic of Korea

[3]School of Chemistry and Chemical Engineering, Yangzhou University, Yangzhou 225009, Jiangsu, P. R. China

[4]Department of Biomedical Engineering, City University of Hong Kong,83 Tat Chee Avenue, Kowloon Tong, Hong Kong

Abstract: Composite hydrogels have gained great attention as three-dimensional (3D) printing biomaterials because of their enhanced intrinsic mechanical strength and bioactivity compared to pure hydrogels. In most conventional printing methods for composite hydrogels, particles are preloaded in ink before printing, which often reduces the printability of composite ink with little mechanical improvement due to poor particle-hydrogel interaction of physical mixing. In contrast, the *in situ* incorporation of nanoparticles into a hydrogel during 3D printing achieves uniform distribution of particles with remarkable mechanical reinforcement, while precursors dissolved in inks do not influence the printing process. Herein, we introduced a "printing in liquid" technique coupled with a hybridization process, which allows 3D freeform printing of nanoparticle-reinforced composite hydrogels. A viscoplastic matrix for this printing system provides not only support for printed hydrogel filaments but also chemical reactants to induce various reactions in printed objects for *in situ* modification. Nanocomposite hydrogel scaffolds were successfully fabricated through this 3D freeform printing of hyaluronic acid (HAc)-alginate (Alg) hydrogel inks through a two-step crosslinking strategy. The first ionic crosslinking of Alg provided structural stability during printing, while the secondary crosslinking of photo-curable HAc improved the mechanical and physiological stability of the nanocomposite hydrogels. For *in situ* precipitation during 3D printing, phosphate ions were dissolved in the hydrogel ink and calcium ions were added to the viscoplastic matrix. The composite hydrogels demonstrated a significant improvement in mechanical strength, biostability, as well as biological performance compared to pure HAc. Moreover, the multi-material printing of composites with different calcium phosphate contents was achieved by adjusting the ionic concentration of inks. Our method greatly accelerates the 3D printing of various functional or hybridized materials with complex geometries through the design and modification of printing materials coupled with *in situ* post-printing functionalization and hybridization in reactive viscoplastic matrices.

Keywords: Three-dimensional freeform printing, *in situ* precipitation, Hydrogels, Nanocomposites, Viscous fluid matrix, Multi-materials

***Corresponding Author:** Juha Song, School of Chemical and Biomedical Engineering, Nanyang Technological University, 70 Nanyang Drive, 637457, Singapore; songjuha@ntu.edu.sg

Received: January 28, 2020**;** ***Accepted:*** March 03, 2020**;** ***Published Online:*** April 02, 2020

Citation: Chen S, Jang TS, Pan HM, *et al*., 2020, 3D Freeform Printing of Nanocomposite Hydrogels through *in situ* Precipitation in Reactive Viscous Fluid., *Int J Bioprint*, 6(2):258. DOI: 10.18063/ijb.v6i2.258.

1 Introduction

Recent advances in three dimensional (3D) printing technologies have facilitated the development of composite biomaterials through the ability to fabricate structurally, functionally, and compositionally intricate constructs[1-4]. Particularly, composite hydrogels have gained a great attention as 3D printing biomaterials

because of their materiality, micro- and macro-structures and functions are comparable to those of biological tissues, with their enhanced intrinsic mechanical strength and bioactivity compared to pure hydrogel systems[5-8] Among various hydrogel systems, hyaluronic acid (HAc)-based composite hydrogels have been applied for tissue scaffolds due to non-immunogenic, biocompatible, and enzymatically biodegradable natures of HAc[9-11]. By incorporating calcium phosphate (CaP), HAc composites exhibited significantly improved mechanical, biochemical, and biological properties, which could be used for dermal fillers or spacers[6,12,13]. Most inorganic-hydrogel composites are printed using composite inks consisting of inorganic particles dispersed in a hydrogel-forming ink before 3D printing[6,7]. This simple mixing approach to prepare composites not only allows easy control over the loading of inorganic particles but is also cell-friendly to enable bioprinting with cells. However, optimizing the printability of the composite inks and print quality often becomes more challenging with increased particle loading. The previous studies have demonstrated that composite inks with only up to 10% nanoparticle loading show suitable printability and structural accuracy. Moreover, the mechanical properties of composite hydrogels depend on the particle-hydrogel interactions and often require an additional modification of either the particles or hydrogels for enhancement of mechanical properties[6].

To overcome these limitations, *in situ* incorporation of nanoparticles has been proposed, whereby permeated ions within the hydrogel structures are reacted by drastically increasing the pH, and nanocrystals are nucleated on the functional groups of the polymer chains within the hydrogels. This *in situ* precipitation method achieves uniform distribution of the nanoparticles, strong particle–polymer bonding, and remarkable mechanical reinforcement in the hydrogel[5,13,14]. One of the possible printing methods to enable *in situ* precipitation-coupled 3D printing is freeform printing in viscous fluid matrices. Freeform 3D printing allows an omnidirectional printing path using mechanically unstable hydrogels with a relatively slow solidification rate[15-19]. Compared with conventional 3D printing in air, embedded freeform 3D printing requires the two shear thinning materials to have matching properties, particularly their shear moduli and shear thinning yield stresses[19,20]. How material parameters influence printability and print quality has been extensively studied[15,20]. Shear thinning of viscous matrices has been achieved by fabricating polymer–nanoparticle composites or dispersing the hydrogel particles in water[15,17,19,20]. Moreover, in addition to the mechanical support provided by the printed soft filaments, a crosslinking agent that induces the solidification of the printed material is often included in the matrix. Alginate (Alg) or silk fibroin-based inks have been successfully printed and crosslinked within hydrogel-based beds for biomedical applications[17,19]. One of the greatest advantages of printing in the liquid is the unique flexibility of the chemical environment. However, despite the revolutionary achievements in freeform printing, viscous fluid matrices have not been used for the functionalization or hybridization of printed materials.

Here, we present a hybridization process for a 3D freeform printing system to fabricate composite hydrogel scaffolds in conjunction with *in situ* precipitation of a mineral phase. By varying the concentration of CaP in a HAc-Alg hydrogel, we developed HAc-Alg/CaP nanocomposite scaffolds with a two-step crosslinking strategy, including physical crosslinking of Alg and photo-crosslinking of glycidyl methacrylate HAc (GM-HAc). To review the effectiveness of our method, we compared the structural compositions, mechanical, physiological, and biological properties between our printed HAc-CaP nanocomposite scaffolds and pure hydrogels or composite hydrogels generated through *ex situ* CaP incorporation. Furthermore, by varying the concentrations of calcium or phosphate ions, multi-material printing of HAc-Alg/CaP with the differing extent of mineralization was achieved with high precision. Taken together, we envisage that our method can accelerate 3D printing using various functional or hybridized materials with complex geometries through the design

and modification of printing materials coupled with *in situ* post-printing functionalization and hybridization in reactive viscoplastic matrices.

2 Materials and methods

2.1 Materials

HAc sodium salt from *Streptococcus equi* (molecular weight ≈ 1.5~1.8 MDa), phosphate-buffered saline (PBS), dimethylformamide (DMF), GM, tetrabutylammonium bromide, triethylamine, acetone, alginic acid sodium salt from brown algae, N-vinylpyrrolidinone (NVP), Irgacure 2959 (2-Hydroxy-4′-(2-hydroxyethoxy) -2-methylpropiophenone), calcium chloride ($CaCl_2$), ammonium phosphate dibasic ($(NH_4)_2HPO_4$), and gelatin from bovine skin (Type B) was purchased from Sigma-Aldrich and used without further purification.

2.2 Preparation of GM-HAc

GM-HAc was synthesized using a previously developed protocol[9]. HAc (1% wt/v) was dissolved in a mixture of PBS and DMF at the volume ratio of 1:1. Then, triethylamine (4.4% v/v), GM (4.4% v/v), and tetrabutylammonium bromide (4.4% wt/v) were added in sequence. After stirring overnight at room temperature, GM-HAc was precipitated with acetone and dissolved in distilled water to remove excess reactants. The solution was dialyzed in distilled water for 2 days, lyophilized, and stored at 4°C. Through the characterization of GM-HAc using nuclear magnetic resonance (Bruker Avance II 300 MHz, Bruker, Germany), the degree of methacrylation was found to be ~15% (**Supplementary Figure 12**).

2.3 Preparation of bulk hydrogel specimens through molding

For the fabrication of HAc-Alg and HAc-Alg/CaP bulk specimens, GM-HAc (1% wt/v) was mixed with Alg (0.125% wt/v), NVP (NVP; 5% v/v), and Irgacure 2959 (1% wt/v) with or without $(NH_4)_2HPO_4$, varying the amount of $(NH_4)_2HPO_4$ from 0.046 M up to 0.092 M, to yield CaP content ranging from 15 to 30 wt%. Then, 1 mL of the resulting solution was transferred to a plastic mold and exposed to ultraviolet (UV) light for 5 min. The gel piece was subsequently physically crosslinked in a 0.153 M $CaCl_2$ solution for 3 h and dialyzed in distilled water for 24 h. To compare composite hydrogels through *in situ* precipitation with those through physically mixing with CaP nanoparticles, CaP nanoparticles were prepared by mixing $CaCl_2$ solution (0.153 M) and $(NH_4)_2HPO_4$ (0.092 M). The CaP precipitate was then centrifuged and lyophilized. GM-HAc (1% wt/v) was mixed with Alg (0.125% wt/v), CaP (0.34% wt/v), NVP (5% v/v), and Irgacure 2959 (1% wt/v). Then, 1 mL of the resulting solution was transferred to a plastic mold and exposed to UV light for 5 min. The gel piece was subsequently physically crosslinked in a 0.153 M $CaCl_2$ solution for 3 h and dialyzed in distilled water for 24 h.

2.4 Preparation of 3D printed hydrogel scaffolds

The gelatin bath was prepared using a previously developed protocol[17]. In brief, gelatin (5% wt/v) was dissolved in a 0.153 M $CaCl_2$ solution at 40°C. The solution was then gelled at 4°C. Subsequently, 5 mL of the gelatin gel and 15 mL of the 0.153 M $CaCl_2$ solution was homogenized at 10,000 rpm for 1 min. The mixture was centrifuged at 4000 rpm for 2 min, and the supernatant was removed to obtain a gelatin slurry support bath.

For 3D printing of HAc-Alg scaffolds, GM-HAc (4% wt/v) was mixed with Alg (0.5% wt/v), NVP (10% v/v), and Irgacure 2959 (2% wt/v) to prepare the ink for 3D printing. The HAc-Alg pure hydrogel scaffold was then printed in the gelatin slurry support bath at a feed rate of 5 mm/s and air pressure of 2.5 bar using a regenHU 3D discovery printer. The scaffold was then exposed to UV light for 5 min and incubated at 37°C to melt and remove the support bath.

For HAc-Alg/CaP composite hydrogel scaffolds, the hydrogel inks were prepared by mixing GM-HAc (4% wt/v) with Alg (0.5% wt/v), NVP (10% v/v), and Irgacure 2959 (2% wt/v) with $(NH_4)_2HPO_4$ (0.092 M) and then printed in the gelatin slurry support bath at a feed rate of 5 mm/s and air pressure of 2.5 bar using the regenHU 3D discovery printer. The scaffold was then exposed

to UV light for 5 min and incubated at 37°C to melt and remove the support bath.

2.5 Characterization of the HAc-Alg and HAc-Alg/CaP hydrogels

HAc-Alg and HAc-Alg/CaP hydrogels were observed using a field emission scanning electron microscope (FE-SEM; Quanta 200F, FEI Company, USA) equipped with energy-dispersive X-ray spectroscopy (EDS). All hydrogel specimens were carefully dried in a three-step process. First, the hydrogels were immersed in a 2.5% glutaraldehyde solution overnight. Subsequently, they were dehydrated using a series of ethanol solutions with the following concentrations: 30%, 50%, 70%, 80%, 90%, 95%, and 100%. Finally, the samples were dried using a critical point dryer (K850, Quorum Technologies, UK). The morphology and chemical composition of precipitated CaP were examined using a transmission electron microscope (TEM; TECHNI G2 ST-F20, FEI, USA) operated at 200 kV acceleration voltage, equipped with EDS. For this analysis, the nanocomposite hydrogels were loaded onto mesh copper grids during the fabrication process and dried in air for 12 h.

The mineral phases of the fabricated hydrogels were analyzed using an X-ray diffractometer (XRD; D/MAX-2500/PC, Rigaku Co., Japan). Three types of the specimen (HAc-Alg and two HAc-Alg/CaP composite hydrogels prepared by physical mixing and *in situ* precipitation) were scanned over a 2θ range of 10 – 70° with a scanning rate of 0.1°/min. The chemical structures of the HAc-Alg and HAc-Alg/CaP scaffolds after degradation were characterized by Fourier-transform infrared (FTIR) spectroscopy (FT-IR; Spectrum One FTIR, PerkinElmer, USA). The amount of CaP incorporated into the nanocomposite hydrogels was measured by thermogravimetric analysis (TGA; STA 409 PC, NETZESCH, Germany). HAc-Alg and HAc-Alg/CaP hydrogels (*in situ* precipitation) were lyophilized and heated at 1000°C at a rate of 5 K/min in nitrogen (N_2) flow.

2.6 Mechanical properties of the HAc-Alg and HAc-Alg/CaP scaffolds

Pieces of HAc-Alg and HAc-Alg/CaP hydrogel fabricated both by mixing and *in situ* precipitation were subjected to rheological tests. All the gel pieces were prepared with a diameter of 25 mm and a thickness of 2 mm. Frequency sweeps were carried out in the angular frequency range of 0.1 – 100 rad/s at 1% strain. Compressive tests of the 3D-printed HAc-Alg and HAc-Alg/CaP porous scaffolds were performed at a strain rate of 10 μm/s up to a predefined strain of 80% using a MicroTester (MTS C42, USA). All of the scaffolds were prepared on a 10 mm × 10 mm × 5 mm scale by 3D printing with or without *in situ* precipitation. The slope of the linear fit for 20 – 30% strain of the stress-strain plot was used as a measurement of the compressive modulus.

2.7 Physiological tests of the HAc-Alg and HAc-Alg/CaP hydrogels

The swelling ratios of HAc-Alg and HAc-Alg/CaP composite hydrogel pieces fabricated with both mixing and mineralization were determined. All of the gel pieces were prepared with a diameter of 25 mm and a thickness of 2 mm. The swelling ratio was evaluated in a PBS solution at 37°C. The gel pieces were lyophilized and weighed to record the initial weight of the dry gel (W_i). They were then immersed in PBS for 24 h and reweighed to record the weight of hydrated gel (W_h). The swelling ratio was calculated according to the equation,

$$\text{Swelling ratio (g/g)} = (W_h - W_i)/W_i \quad (1)$$

HAc-Alg and HAc-Alg/CaP hydrogel scaffolds were prepared by 3D printing and used for degradation tests. All of the scaffolds were prepared with dimensions of 10 mm × 10 mm × 5 mm. The scaffolds were immersed in a PBS solution at 37°C with hyaluronidase at a concentration of 100 – 250 UI/ml. The degradation rates were investigated by measuring the weight changes as follows:

$$\text{Remaining weight (\%)} = (W_r/W_i) \times 100 \quad (2)$$

where W_r is the remaining weight and W_i is the initial weight.

2.8 *In vitro* cytotoxicity test

HAc-Alg and HAc-Alg/CaP hydrogel pieces cast in plastic molds were used for the cell viability tests. All of the gel pieces were prepared in 12-well plates. The fibroblast cell line L929 (a derivative of *Mus musculus* strain L) was used to assess the cellular responses to the hydrogels. Before seeding, the samples were washed with Dulbecco's PBS and then sterilized under UV irradiation for 1 h. The cells were seeded at a density of 5×10^4 cells/mL. They were cultured in minimum essential medium (MEM)-alpha medium with 10% fetal bovine serum (FBS) and 1% penicillin-streptomycin in an incubator with 5% CO_2 at 37°C. Cell viability was tested via the AlamarBlue assay after 3 and 5 days of culturing. Cellular morphology on the surfaces of both hydrogel specimens was observed using FE-SEM (FE-SEM; Quanta 200F, FEI Company, USA) after 5 days of culturing. All of the samples were washed 3 times using PBS. They were then fixed in 2.5% glutaraldehyde solution and were gradually dehydrated with a series of ethanol solutions with the following concentrations: 30%, 50%, 70%, 80%, 90%, 95%, and 100%.

For cell attachment tests of 3D-printed composite hydrogels, fluorescence microparticles (FluoSpheres carboxylate-modified microspheres, 1.0 μm, blue fluorescent [350/440], Invitrogen, Thermo Fisher Scientific, USA) were incorporated into the inks to stain the printed scaffolds for imaging. The cells were seeded at a density of 5×10^5 cells/ml and cultured for 7 days. The cells were stained with nucleic acid stain (Hoechst 33342, trihydrochloride, trihydrate, Invitrogen, Thermo Fisher Scientific, USA) and plasma membrane stain (CellMask, deep red plasma membrane stain, Invitrogen, Thermo Fisher Scientific, USA). Cell adhesion was observed using a confocal laser scanning microscope (CLSM, LSM 800, ZEISS, Germany).

For the cell viability test of cell-laden HA-Alg porous scaffolds, pure hydrogel inks consisting of 4% w/v GMHA, 0.5% w/v Alg, 0.5% v/v NVP, 0.9% w/v NaCl, and 0.5% w/v Irgacure 2959 were prepared for 3D printing. Cell-laden Alg microparticles with a cell density of 6×10^6 cells/ml were prepared as previously described Pan *et al*.[21] The cell-laden microparticles were mixed with the HA-Alg ink at a mass ratio of 1:3. The cell-laden inks were printed in the gelatin slurry support bath at a feed rate of 5 mm/s and air pressure of 0.5 bar using the 3D printer with a 0.51 mm nozzle. The printed scaffolds were then exposed to UV light for 2.5 min and incubated at 37°C to melt and remove the support bath. All of the cell-laden scaffolds were the washed 3 times with PBS to remove any remaining gelatin and were then incubated with live/dead staining solution containing 2 μM calcein-AM and 4 μM ethidium homodimer-I stains for 30 min at 37 °C. The stained cells were observed using CLSM (LSM 800, ZEISS, Germany).

2.9 *In vitro* differentiation test

Osteogenic differentiation was evaluated using MC3T3-E1 pre-osteoblast cells cultured in MEM-alpha medium (no ascorbic acid, Gibco, Thermo Fisher Scientific, USA) with 10% FBS and 1% penicillin and streptomycin in an incubator with 5% CO_2 at 37°C. The cells were seeded at a density of 2×10^5 cells/well on a 12-well plate for the control and 1×10^6 cells/scaffold for the HAc-Alg/CaP composite hydrogel scaffolds. They were cultured in either cell maintenance medium or osteogenic medium (cell maintenance medium supplemented with 0.05 mg/mL ascorbic acid and 10 mM β-glycerophosphate) for 2 weeks. Gene expression was evaluated by quantitative real-time polymerase chain reaction (qPCR) after 14 days of culturing. RNA was extracted from the cells by TRIzol (Invitrogen, Thermo Fisher Scientific, USA) and then converted to cDNA through reverse transcription by Moloney Murine Leukemia Virus reverse transcriptase (Promega, USA). To test *in vitro* cell differentiation, the following four markers, Runx2, Collagen type 1 (COL1), osteopontin (OPN), and osteocalcin (OCN), were chosen, while actin was used as a reference gene [ref]. The sequences of each gene are shown in **Table 1**. The qPCR was conducted using a CFX Connect real-time system (Bio-Rad, USA) with SsoAdvanced Universal SYBR Green

Table 1. Sequence of primers for the RT-qPCR.

Gene	Forward primer sequence	Reverse primer sequence
Actin	5'-GTGCTATGTTGCCCTAGACTTCG-3'	5'-GATGCCACAGGATTCCATACCC-3'
Col 1	5'-CAAGATGTGCCACTCTGACT-3'	5'-TCTGACCTGTCTCCATGTTG-3'
RunX2	5'-GCATGGCCAAGAAGACATCC-3'	5'-CCTCGGGTTTCCACGTCTC-3'
OCN	5'-CTTTCTGCTCACTCTGCTG-3'	5'-TATTGCCCTCCTGCTTGG-3'
OPN	5'-CACTTTCACTCCAATCGTCCCTAC-3'	5'-ACTCCTTAGACTCACCGCTCTTC-3'

RT-qPCR: Quantitative real-time polymerase chain reaction, OCN: Osteocalcin, OPN: Osteopontin

Supermix (Bio-Rad, USA). For analysis, the gene expression values were first normalized to the reference gene (Actin) and then normalized to the control group in cell maintenance medium.

2.10 3D printing of multiphase HAc-CaP scaffolds

HAc-Alg/10wt% CaP and HAc-Alg/30 wt% CaP composite hydrogel inks were prepared, as described in the previous section. Both hydrogel inks were preloaded into the cartridge before 3D printing. For the vertical stacking scaffold, six layers of HAc-Alg/30 wt% CaP ink were first extruded into the gelatin bath. Then, the cartridge was changed and six layers of HAc-Alg/10 wt% CaP ink were printed on top of the printed structure. For horizontal stacking, six layers of HAc-Alg/10 wt% CaP were first printed to form an inner core structure. Subsequently, the HAc-Alg/30 wt% CaP ink was extruded, surrounding the inner structure to create the outer shell part. Subsequently, post-curing with UV irradiation was performed to stabilize the multi-material scaffolds.

2.11 Statistical analysis

All experimental results were presented as mean ± standard deviation (SD) for $n \geq 3$. One-way analysis of variance was used to determine the difference between groups, and $P < 0.05$ was considered statistically significant.

3 Results and discussion

3.1 3D freeform printing of composite hydrogels

To enable *in situ* precipitation of CaP during 3D printing of HAc filaments, we considered two key issues. First, for *in situ* precipitation, it is necessary to incorporate calcium and phosphate ions into the hydrogel ink and the supportive viscous fluid matrix, respectively. Second, *in situ* precipitation should not inhibit either the crosslinking of the printed hydrogel filaments or interlayer bonding between the printed layers. To resolve these two issues, HAc-Alg hydrogels were used for dual crosslinking in conjunction with *in situ* CaP precipitation (**Figure 1**). The first physical crosslinking of Alg was induced within a gelatin-based viscoplastic matrix containing excess calcium ions, while the *in situ* precipitation occurred throughout the printed filaments. The crosslinked Alg maintained the structural integrity of the printed filaments within the fluid during the reaction. Pure HAc hydrogels were also printed to compare with HAc-Alg hydrogels. The printed structure of HAc hydrogels could not be well-maintained inside the gelatin slurry since the inks remained unsolidified. As a result, the printing quality of pure HAc scaffolds is significantly lower than that of HAc-Alg. Moreover, the printed HAc scaffolds were mechanically weak. The storage modulus of HAc hydrogels was one order of magnitude smaller than that of HAc-Alg hydrogels (**Supplementary Figure 7-A**). Thus, we clearly confirmed that the physical crosslinking process with Alg significantly improves the mechanical stability of printed HAc hydrogels during printing and even after UV crosslinking.

After the completion of 3D printing, the mineralized scaffold was irradiated with UV for 10 min. The photocrosslinking of GM-HAc caused complete solidification of the entire scaffold, which increased the mechanical and chemical stability of the hydrogel. The Alg/HAc ratio was optimized to moderate the onset of the sol-gel transition of HAc-Alg after the physical crosslinking of the Alg. The printability of hydrogel-forming inks and the

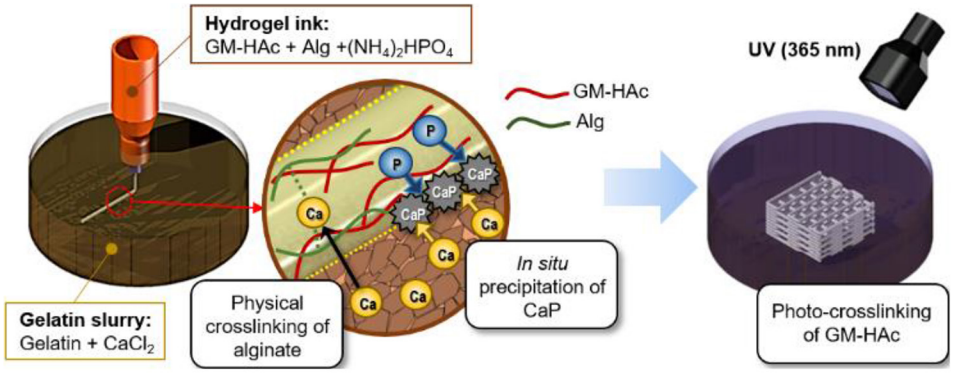

Figure 1. Schematic of three-dimensional freeform printing system of nanocomposite hydrogels through a two-step crosslinking process coupled with *in situ* precipitation.

interlayer bonding of mineralized filaments were markedly influenced by the amount of crosslinked Alg within the HAc-Alg during 3D printing. The optimal Alg/HAc ratio was found to be 1:8.

The ink composed of GM-HAc and Alg with $(NH_4)_2HPO_4$ is extruded into a gelatin supporting bath with $CaCl_2$. Physical crosslinking of Alg and *in situ* precipitation of CaP take place simultaneously during the 3D printing process. The printed construct is post-treated with photocrosslinking by UV irradiation. The amount of precipitated CaP is controlled by varying the concentration of $(NH_4)_2HPO_4$ in ink.

The 3D hydrogel structures were fabricated within a supportive viscous fluid matrix composed of gelatin microparticles and calcium chloride[17]. As the rheological behavior of gelatin is affected by pH, HAc-Alg solutions with phosphate (PO_4^{3-}) ions are required to be at pH 7 – 8 to achieve good print quality. We used diammonium hydrogen phosphate (diammonium phosphate [DAP]) instead of phosphoric acid to facilitate the reaction described by Eq. (3), aiming to obtain dicalcium phosphate dehydrate ($CaHPO_4{\cdot}2H_2O$, dicyclopentadiene [DCPD]), which is known to be a common precursor of hydroxyapatite[13,22].

$$(NH_4)_2HPO_4 + CaCl_2 \rightarrow CaHPO_4{\cdot}2H_2O + 2NH_4 + 2Cl^- \quad \text{at pH 8, 25°C} \qquad (3)$$

It is noteworthy that the rheological properties of inks for both HAc-Alg and HAc-Alg/CaP hydrogels are almost identical regardless of the existence of phosphate ions. Thus, the printing parameters for both inks were exactly the same, without additional optimization depending on mineral contents of inks since the particles post-loaded into the hydrogel should not hinder the printing process.

Figure 2 shows both pure and composite hydrogels printed with ten layers. The transparency of the printed scaffolds was used as an indicator of mineral incorporation (**Supplementary Videos 1 and 2**). The lateral view optical images of the printed porous scaffolds exhibited an almost circular cross-sectional area regardless of the material composition. During the UV treatment, gelatin microgels became fully fluidized due to the heat generated from the crosslinking reactions, thereby releasing the solidified printed objects (**Supplementary Videos 3 and 4**). Moreover, we printed composite hydrogels on a glass slide without any supporting matrix (**Supplementary Figure 1**). The printed structure of the hydrogels was almost collapsed due to lack of self-supportability. Therefore, printing in liquid clearly improved printability of soft materials with good printing quality in addition to functionalization of printed materials.

3.2 Structural characterization of the printed scaffolds

After critical point drying, the surface and cross-sectional morphologies of the printed scaffolds were observed using SEM (**Figure 3**). While pure hydrogel scaffolds exhibited macroscopically rough and porous surfaces, mineralized composite

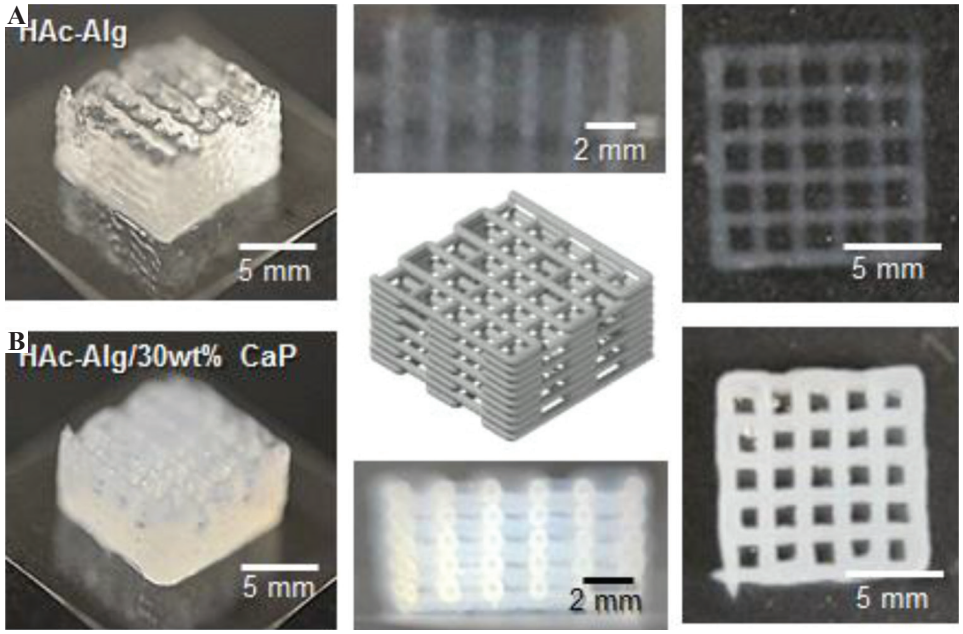

Figure 2. Schematics and optical images of three-dimensional-printed scaffolds. (A) Hyaluronic acid-alginate (HAc-Alg) hydrogel scaffolds (perspective view, top view, and side view). (B) HAc-Alg/30 wt% calcium phosphate composite hydrogel scaffolds (perspective view, top view, and side view).

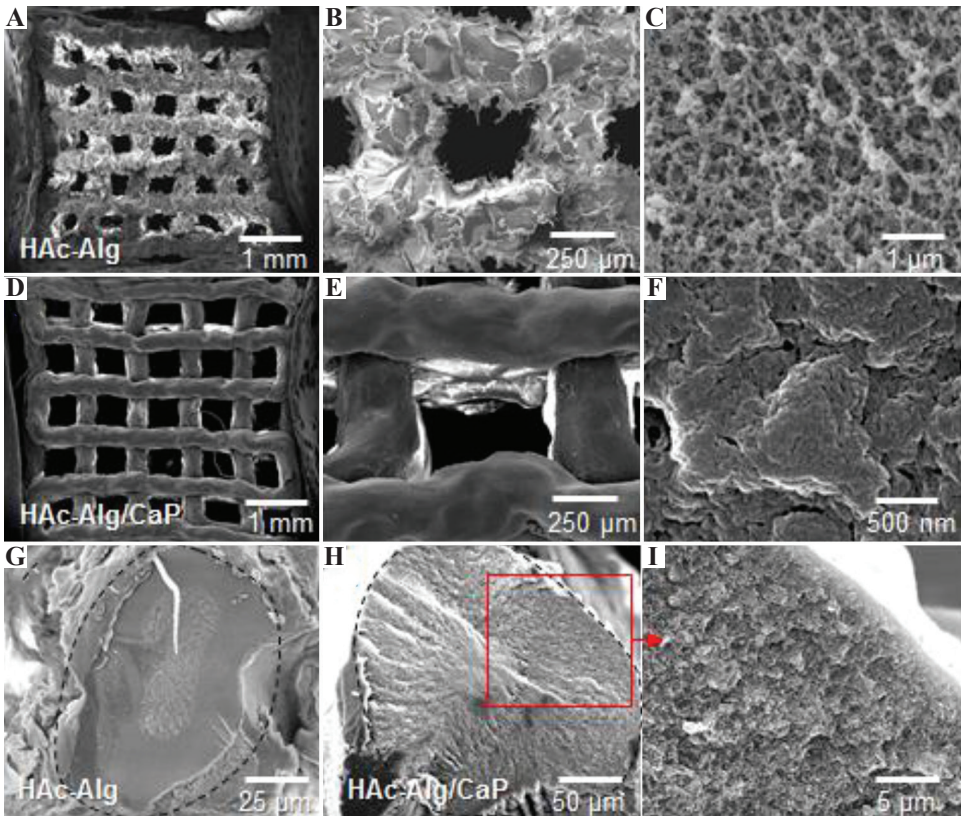

Figure 3. Surface and cross-sectional morphologies of dehydrated 3D-printed scaffolds. (A-C) Surface morphology of hyaluronic acid-alginate (HAc-Alg) hydrogel scaffolds. (D-F) Surface morphology of HAc-Alg/30 wt% calcium phosphate (CaP) composite hydrogel scaffolds. (G) Cross-sectional morphology of a printed HAc-Alg filament. (H and I) Cross-sectional morphology of a printed HAc-Alg/30 wt% CaP filament.

scaffolds exhibited smooth and dense surfaces (**Figure 3A-F**). The high-resolution SEM image of HAc-Alg indicated the presence of spherical nanoparticles with sizes ranging from five to a few tens of nanometers on the nanoporous polymeric network (**Figure 3C**). In contrast, the HAc-Alg/CaP hydrogel exhibited densely packed nanoparticles that formed a continuous mineral network throughout the printed scaffold (**Figure 3D**).

The increased CaP content (from 10 wt% to 30 wt%) was caused by the increased number of CaP particles and not the crystal growth of nanoparticles (**Supplementary Figure 2 and Supplementary Table 1**). The nucleation rate of nanoparticle formation is often experimentally described in terms of supersaturation of the solution (S), free surface energy (γ) of particles and temperature (T) as follows, where A and C are constants[23]:

$$\frac{dN}{dt} = Aexp(C \bullet \frac{\gamma^3}{T^3 (lnS)^2}) \quad (4)$$

According to Eq. (4), the total number of CaP nuclei should be significantly larger for 30 wt% CaP compared with 10 wt% CaP at room temperature, due to the higher level of supersaturation induced by increased phosphate ions in the presence of excess calcium ions (assuming that the CaP of both systems has the same free surface energy)[23]. Meanwhile, the total reaction time was limited to 20 min, which constrained the growth of nanoparticles. As a result, CaP nanoparticles for HAc-Alg/30 wt% CaP formed the continuous inorganic phase through the aggregation of densely packed nano-precipitates, which uniformly coated the surface of the polymer matrix, reducing the surface roughness (**Figure 3E and F**).

We presumed that the obtained mineral phase was mainly DCPD based on the chemical reaction, as shown in Eq. (3). To analyze the mineral phase of the composite hydrogels, the nanocrystals were characterized using TEM, X-ray diffraction, and EDS. The XRD pattern of HAc-Alg revealed the existence of calcium carbonate nanocrystals (**Figure 4A**). These nanoparticles were either vaterite or calcite. In a Ca^{2+}-gelatin bath, HAc-Alg undergoes ionic crosslinking, whereby calcium carbonate is formed through the reaction between calcium and carbonate ions. Carbonate ions are known to exist in aqueous solution due to the dissolved carbon dioxide[24]. Hosoda and Kato previously demonstrated the formation of a thin calcium carbonate crystalline layer in a reactive Ca^{2+}-containing solution in the presence of insoluble and soluble acidic polymers with carboxyl groups[25]. The HAc-Alg units inside the gelatin bath should act as insoluble acidic polymers and soluble acidic biomacromolecules, allowing calcium carbonate crystals to grow on the polymer matrix. Due to the interactions between the calcium ions and carboxyl groups, the localized calcium concentration around the HAc-Alg matrix is likely to induce crystal growth.

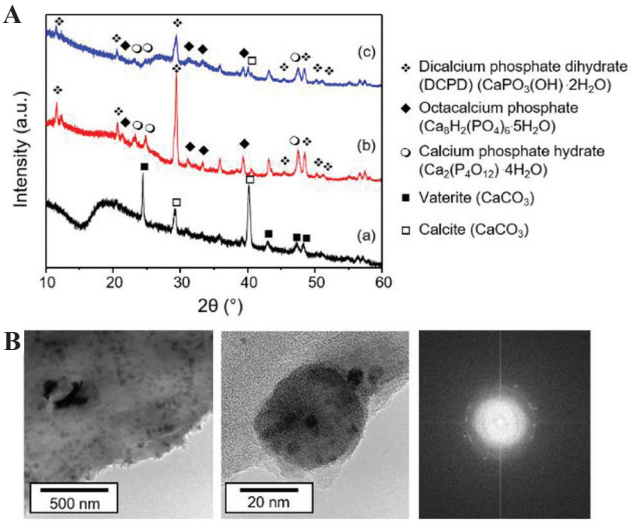

Figure 4. Mineral phases of hyaluronic acid-alginate (HAc-Alg)/calcium phosphate (CaP) hydrogels. (A) X-ray diffractometer patterns of (a) HAc-Alg hydrogels, (b) HAc-Alg/30 wt% CaP composite hydrogels prepared by mixing, and (c) HAc-Alg/30 wt% CaP composite hydrogels prepared by *in situ* precipitation. (B) Transmission electron microscope images of CaP nanoparticles in HAc-Alg/CaP composite hydrogels (prepared by *in situ* precipitation) and corresponding selected-area electron diffraction patterns of CaP nanoparticles.

The XRD patterns of two HAc-Alg/CaP composite specimens prepared by *ex situ* incorporation and *in situ* precipitation were almost identical, implying that the existence of the polymer template did not alter the CaP phases. The dominant CaP nano-precipitates were DCPD crystals. We also identified other CaP precipitates such as octacalcium phosphate (OCP) and CaP hydrate with a small amount of calcite. For a clearer observation of the CaP nanoparticles formed on HAc-Alg, a ten-fold diluted HAc-Alg ink with DAP solution (to maintain the ionic concentrations) was used. The increased pore size due to the lower polymer concentration prevented cohesive agglomeration of the CaP precipitates. The TEM revealed uniform spherical nanoparticles of ~60 nm, which was consistent with the morphology of CaP on HAc-Alg obtained using SEM. The selected area electron diffraction (SAED) pattern of the CaP nanoparticles indicated a characteristic polycrystalline ring, which correlated with the multiple characteristic peaks in the XRD pattern. EDS mapping of the composite hydrogels confirmed that these nanoparticles were composed of calcium, phosphorus, and oxygen (**Supplementary Figures 3-5**). As expected, the quantitative EDS analyses indicated that the nanocrystals contained 10 at.% Ca, 17 at.% P, and 73 at.% O (a Ca/P ratio of ~0.6). As the Ca/P ratios of OCP, DCPD, and CaP hydrate were 1.33, 1, and 0.5, respectively, the quantified Ca/P ratio indicated that the CaP nanocrystals were a mixture of OCP, DCPD, and CaP hydrate.

The weight fraction of inorganic nanoparticles in the printed hydrogels was determined using TGA (**Supplementary Figure 6**). The TGA result for the HAc-Alg scaffold indicated that the weight fraction of calcium carbonate was ~5 wt% before the decomposition of calcium carbonate to calcium oxide above 600°C[26]. In contrast, the weight fractions of calcium carbonate and CaP for HAc-Alg/CaP scaffolds were estimated to be ~4 and ~32 wt%, respectively. The desired mineral content could be achieved solely through *in situ* precipitation during 3D printing. The size of the mineral particles observed in this study (~60 nm) was much smaller than that observed in our previous study (200~350 nm), where the CaP content of the HAc-CaP bulk hydrogels fabricated by *in situ* precipitation was influenced by the size of the CaP nanoparticles[5]. Instead, the increased phosphate concentration in the presence of excess calcium ions is likely to have accelerated the nucleation rate of CaP nanoparticles (**Supplementary Table 2**)[23]. As the total precipitation time of our system was limited to 20 min, the average sizes of nanoparticles were almost identical regardless of the mineral contents in the HAc-Alg/CaP hydrogels **(Supplementary Figure 2 and Supplementary Table 2**). Taken together, our results indicate that the mineral content of HAc-Alg/CaP hydrogels can be effectively modulated by varying the phosphate concentration in the inks.

3.3 Mechanical behavior of the composite gels and scaffolds

Hydrogels are often regarded as soft materials that are not suitable for various load-bearing conditions. Thus, nanocomposite biomaterials are more suitable to be used as various tissue scaffolds or fillers that require structural integrity and mechanical stability during cell proliferation and differentiation[5,7,14,27]. To compare the mechanical properties of the different composite hydrogels and pure hydrogels, various mechanical tests were performed (**Table 2**). Rheological tests on bulk hydrogels revealed that the storage moduli of the HAc-Alg/CaP nanocomposite hydrogels were 4 times higher than those of the HAc-Alg hydrogels (**Supplementary Figure 7-B**). Furthermore, significant differences were found in all pair-wise comparisons conducted between the HAc-Alg/30 wt% CaP generated by *in-situ* precipitation and HAc-Alg/30 wt% CaP generated by *ex situ* incorporation, indicating that the HAc-Alg/30 wt% CaP generated by *in situ* precipitation exhibited a remarkable improvement in mechanical and swelling behaviors compared with the HAc-Alg/30 wt% CaP generated by *ex situ* incorporation. We also fabricated HAc-Alg and HAc-Alg/CaP scaffolds using a 3D printer and measured their local and global mechanical properties. In fact, the composite HAc-Alg/30

Table 2. Mechanical behavior of fully hydrated HAc-Alg hydrogels, and HAc-Alg/ 30wt% CaP composite hydrogels prepared by mixing and *in situ* precipitation (n>3).

Specimen	Swelling ratio (g/g)	Bulk gel[a]	3D printed porous scaffold	
		G' (Pa)[b]	E (kPa)	σ_c (kPa)[c]
HAc-Alg	31±2	298±58	3.3±0.6	18.9±2.1
HAc-Alg/30wt% CaP (mixing)[d]	28±1	502±62	N.A.	N.A.
HAc-Alg/30wt% CaP (*in situ precipitation*)	25±1	1397±194	6.4±1.2	35.9±2.9

[a]hydrogel specimens fabricated by direct casting using a cylindrical mold and assessed by a rheometer, [b]storage modulus at frequency of 1 Hz, [c]maximum stress at compressive strain, ε=0.8, [d]HAc-Alg/ 30wt% CaP ink prepared by mixing CaP with HAc-Alg has very low printability due to high viscosity and inconsistent extrusion behavior; thus, its 3D printed scaffolds could not be fabricated for mechanical tests. HAc-Alg: Hyaluronic acid-alginate, CaP: Calcium phosphate, 3D: Three-dimensional

wt% CaP inks prepared by *ex situ* incorporation could not be printed due to severe clogging issues associated with high viscosity and particle agglomeration. Thus, only HAc-Alg/CaP scaffolds prepared by *in situ* precipitation were used in our mechanical tests.

Next, we performed unconfined, uniaxial compression test to assess the mechanical characteristics of the printed scaffolds under significant deformation conditions using fully hydrated HAc-Alg and HAc-Alg/CaP scaffolds (**Table 2 and Supplementary Figure 7-C**). Under a predefined deformation (ε = 80%), the rods and struts of both HAc-Alg and HAc-Alg/CaP hydrogels were crushed, and the porous scaffolds subsequently densified. Both scaffolds did not collapse until the predefined deformation point (ε = 80%) with significant densification. All specimens maintained their structural integrity after unloading. The incorporation of 30 wt% CaP precipitates in the hydrogels resulted in a two-fold enhancement of the compressive modulus and strength (**Table 2**). The precipitated CaP minerals improve the chain stiffness of the polymer networks due to (i) the strong electrostatic interactions between the minerals and carboxyl groups of the polysaccharide chains and (ii) homogeneous distribution of the minerals as opposed to the case of simple mixing[5,28]. Notably, the enhancements of compressive stiffness and strength in composite hydrogel scaffolds were not as striking as the enhancements in storage moduli of bulk gels and local stiffness of individual struts in the scaffolds. We speculated that this was due to the high porosity and structural instability associated with irregular, inhomogeneous pore structures of porous scaffolds, which counteracted mechanical enhancement[29]. In this study, we clearly demonstrated that *in situ* precipitation of CaP better enhanced the mechanical properties of the hydrogel composites compared with using *ex situ* CaP incorporation.

One of the advantages of our approach is that the printed hydrogels were not deformed in water due to the pre-swelling condition associated with 3D freeform printing in an aqueous medium. The swelling ratios of the printed hydrogels were studied within 24 h of the printing and subsequent post-UV curing processes (**Table 2 and Supplementary Figure 7-D**). In all cases, the equilibrium swelling ratios were almost reached, indicating that the HAc-Alg/CaP nanocomposite hydrogels exhibited reduced swelling ratios due to the increased chain stiffness and crosslinking density of the mineralized hydrogels[5,30]. During the printing of multiphase hydrogel composites with gradient compositions, one of the key concerns is the mismatch of swelling ratios among various gradient hydrogel materials after printing, as this can lead to significant structural distortion and structural instability of the printed constructs. Printing in a water-based slurry system can minimize any such issues associated with the swelling behavior of multiphase hydrogel systems.

3.4 *In vitro* biostability of the composite scaffolds

Enzymatic degradation of HAc often results in low biostability of the HAc-based scaffolds and requires physical or chemical crosslinking of the functionalized HAc. The *in vitro* biostability of the 3D printed hydrogels was evaluated in the presence

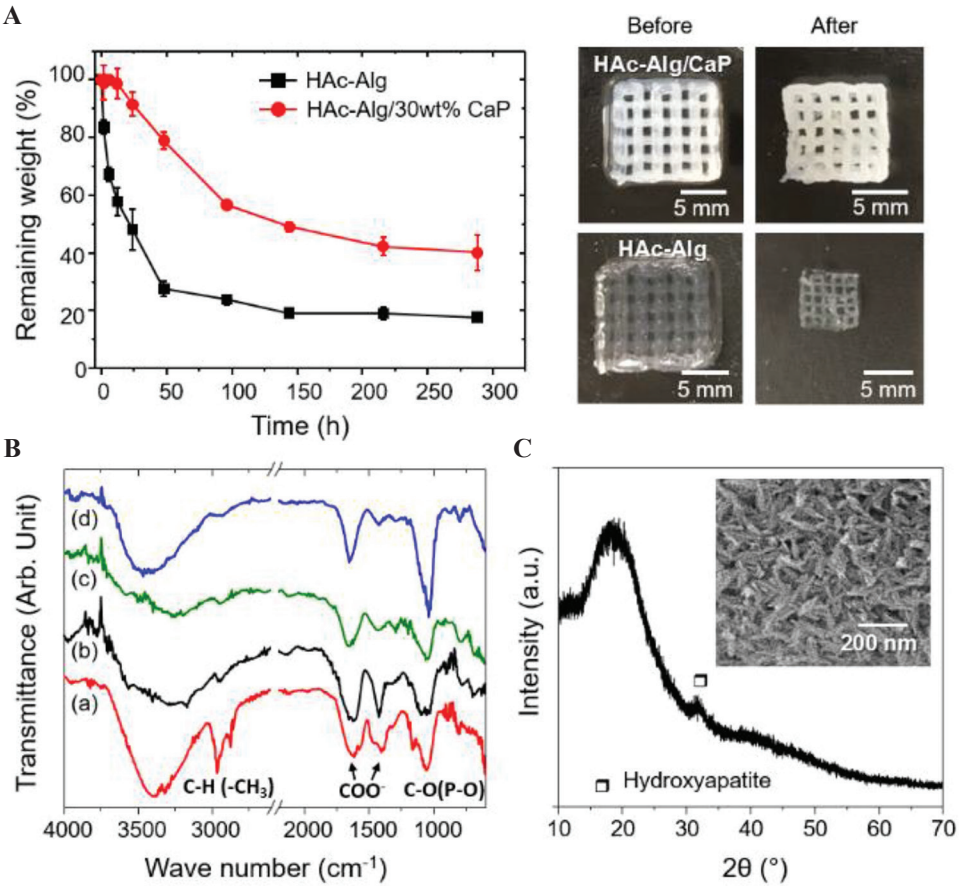

Figure 5. *In vitro* enzymatic degradation behavior of three-dimensional-printed scaffolds. (A) Remaining weight over incubation time after the hydrogel scaffolds were immersed in hyaluronidase solution, and optical images of the scaffolds before and after enzymatic degradation. (B) Fourier-transform infrared spectra of (a) glycidyl methacrylate-hyaluronic acid (HAc) hydrogel, (b) alginate hydrogel, (c) HAc-alginate (HAc-Alg) after degradation, and (d) HAc-Alg/30 wt% calcium phosphate (CaP) after degradation. (C) X-ray diffractometer pattern of HAc-Alg/30 wt% CaP scaffolds after degradation.

of hyaluronidase through a 7-day immersion study (**Figure 5A**). We found that approximately 85% of HAc in the HAc-Alg scaffolds was rapidly degraded after 2 days, whereas >50% of HAc remained in HAc-Alg/CaP, indicating that the nanocomposite hydrogels exhibited higher resistance against enzymatic degradation. The complete degradation of HAc in HAc-Alg and HAc-Alg/CaP took 6 and 12 days, respectively (**Supplementary Figure 8**). The optical images of the remnant hydrogels after degradation confirmed the outstanding biostability of the HAc-Alg/CaP hydrogels. The precipitation of nanocrystals on the HAc chains effectively blocked the access of enzyme molecules to HAc and enhanced its resistance to enzymatic degradation[5,31].

Our results indicate that Alg and minerals were the main components of the remaining scaffolds after hyaluronidase-mediated degradation, as confirmed by the FT-IR spectra (**Figure 5B**). The FT-IR spectra of GM–crosslinked HAc and Alg hydrogels had the following characteristic peaks: For GM–crosslinked HAc, amide N-H stretch from 3200 to 3600 cm^{-1}, C=O stretching and N–H bending in the 1595 – 1710 cm^{-1} range, C–H bending peak between 1350 and 1480 cm^{-1}, and C–O stretch of the proteoglycan sugar ring from 985 to 1140 cm^{-1}; and for Alg, stretching vibrations of the hydroxyl groups at 3430 cm^{-1} and stretching vibrations of the asymmetric and symmetric bands of carboxylate anions at 1619 and 1416 cm^{-1}, respectively[32,33]. The FT-IR

spectrum of degraded HAc-Alg was in line with that of Alg. In contrast, characteristic peaks of CaP were observed in addition to those of Alg for the HAc-Alg/CaP hydrogels: The FT-IR spectrum exhibited strong peaks at 1000 – 1100 cm^{-1} (ν3 bending) and 560 – 600 cm^{-1} (ν4 bending) for the PO_4^{3-} groups in addition to the bands of adsorbed water from 3600 to 2600 cm^{-1}[34]. We also observed significant discrepancies between the remaining weight obtained from the TGA analysis and enzymatic degradation tests. While the remaining weight of TGA analysis accounted for residual organic ashes and inorganic components, the remaining weight after enzymatic degradation was mainly due to swollen Alg (Alg + water) and inorganic components such as calcium carbonate and CaP. Moreover, the swelling behavior of the remaining Alg hydrogels varied depending on the mineral contents of the composite hydrogels (**Table 2**)[5]. The remaining weight difference between degraded HAc-Alg and HAc-Alg/CaP scaffolds was ~20 wt%, which was <30 wt% obtained from the TGA analysis.

HAc-Alg/CaP hydrogels after 2 weeks of immersed degradation were also analyzed using XRD and SEM to determine the mineral phases of CaP. A broad peak at 32−35° indicating apatite with low crystallinity was observed in the XRD pattern, while the characteristic peaks of DCPD or OCP crystallites had completely disappeared (**Figure 5C**). Furthermore, the morphology of the CaP precipitates changed from spherical to needle-like (**Supplementary Figure 9**). It is known that DCPD, one of the CaP crystalline phases found in HAc-Alg/CaP scaffolds, can be hydrolyzed in water or a buffer solution to form hydroxyapatite or anhydrous dicalcium phosphate[22].

$$5CaHPO_4 + H_2OHaH_5(PO_4)_3\,OH + 2H_3\,PO_4 \qquad (5)$$

In this hydrolytic reaction, the acidic by-product decreases the pH of the aqueous medium. We, therefore, used a PBS buffer solution in our degradation test to minimize the pH change of the system. The final pH of the enzymatic solution was around 7, which was slightly lower than the initial pH (pH 7.4). Through heat treatment, pure ceramic porous scaffolds could be obtained after the removal of the Alg remnants, with the crystallization of amorphous apatite phases.

In addition to confirming the improved biostability of HAc-Alg/CaP, two promising findings were discovered from our degradation tests. First, the precipitated minerals were well-connected with the polymer template and maintained their 3D structure after template removal. Thus, by developing an *in situ* precipitation method for nanoparticles, various minerals can be incorporated in the 3D printing process to obtain porous 3D foams of metals or ceramics. For example, gold nanoparticles can be nucleated and grown on a polymer matrix through the *in situ* reaction of its metal precursor (e.g., $HAuCl_4$) and a reducing agent (e.g., HCOONa)[35,36]. Second, by employing additional post-treatment processes, 3D printed materials can be further modified (e.g., by reduction of metal oxides)[37]. Importantly, this freeform 3D printing allows polymer templates to be chosen based on their functional roles instead of their 3D printability as the gelation of the polymer templates is carried out after 3D printing.

3.5 Biological performance of composite hydrogels

The biocompatibility and bioactivity of HAc-Alg/CaP were carefully evaluated and compared to that of HAc-Alg to confirm its potential as a biomaterial for various medical applications. The *in vitro* cellular responses of fibroblast cells on the bulk and 3D-printed hydrogels are shown in **Figure 6**. None of the hydrogels displayed any signs of cytotoxicity. The cells attached to the surface of HAc-Alg/CaP bulk hydrogels appeared stretched and flattened, similar to what is usually observed in two-dimensional cell cultures. In contrast, the cells attached to the surface of HAc-Alg hydrogels clustered to form spheroids (**Figure 6A**). The cell densities were remarkably higher on HAc-Alg/CaP surfaces than on HAc-Alg surfaces. After a 3-day culture, 80 – 90% of the HAc-Alg/CaP surface area was covered by the cells, whereas only ~20% of the HAc-Alg surface area was occupied by the cells (**Supplementary**

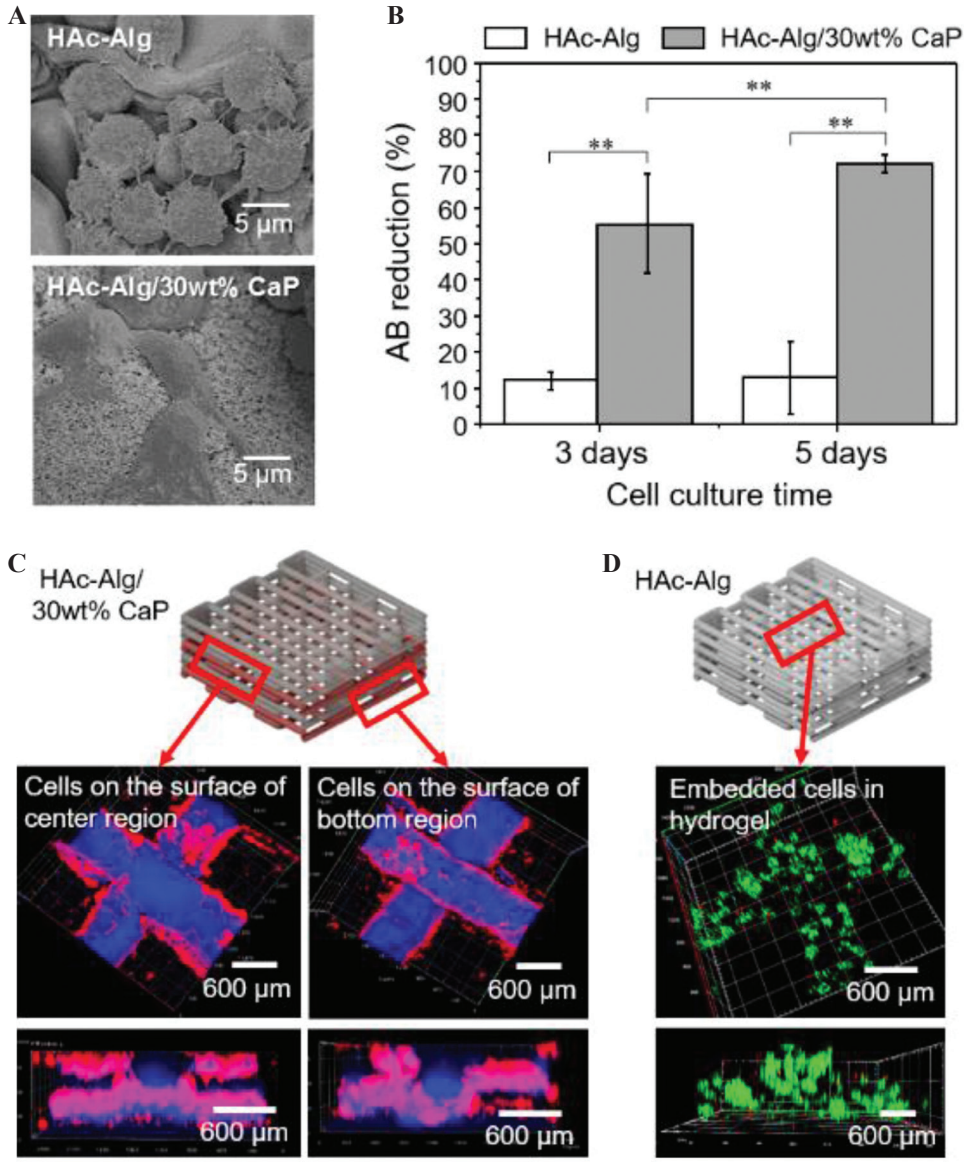

Figure 6. Cytocompatibility of hyaluronic acid-alginate (HAc-Alg) and HAc-Alg/30 wt% calcium phosphate (CaP) hydrogels using L929 fibroblasts. (A) Scanning electron microscope images of cells attached to the surfaces of HAc-Alg and HAc-Alg/30 wt% CaP hydrogels. (B) Cell viability of HAc-Alg and HAc-Alg/30 wt% CaP hydrogels measured by AlamarBlue assay after 3 and 5 days ($n > 3$, $^{**}P < 0.01$). (C) Confocal laser scanning microscope (CLSM) z-stack images of L929 fibroblasts adhered to HAc-Alg/30wt% CaP three-dimensional (3D) scaffolds after 7 days, indicating the selected parts for imaging. The two layers from the bottom and center regions were imaged to confirm the cell distribution throughout the scaffold. (D) CLSM z-stacked confocal images of L929 fibroblasts within the 3D printed scaffold after a 14-day incubation period.

Figure 10). This observation agreed well with the quantitative cell proliferation data obtained using the AlamarBlue assay (**Figure 6B**). The levels of fibroblast proliferation on the HAc-Alg/CaP hydrogels after 3 and 5 days of culture were, respectively, ~6 and 8 times higher than those on HAc-Alg. The relatively high SD in HAc-Alg on day 5 was due to the weak cell attachment on the hydrogel surface, whereas the higher SD for the HAc-Alg/CaP hydrogels was attributed to errors

in cell seeding. When the cell densities reached saturation on day 5 (almost covering the entire surface of the composite hydrogel), the errors were <5%. In most cases, CaP-containing biomaterial scaffolds promote cell growth[5,38,39]. DCPD-based brushite cements are non-inflammatory and biocompatible with both bone and soft tissues[40]. Moreover, the nanosized surface topography and improved matrix stiffness associated with the incorporated CaP precipitates may provide physical binding sites and stable mechanical support for the seeded cells[14,39].

Based on the observations of HAc-Alg and HAc-Alg/CaP bulk hydrogels, we found that different types of hydrogel scaffolds required different cell seeding strategies. In the case of 3D printed HAc-Alg/CaP scaffolds that exhibited excellent cell attachment performance, cells were directly seeded on the scaffolds after all of the processing steps were completed. The cell growth on 3D printed HAc-Alg/CaP was examined using CLSM. We found that cells migrated inside the pore channels of the hydrogel scaffold and almost fully covered the 3D surface (**Figure 6C**). As cells seeded on HAc-Alg attached and proliferated poorly, cell-laden HAc-Alg scaffolds were prepared and incubated for 14 days (**Figure 6D**). The encapsulated cells observed using CLSM were highly viable. For printing with cell-laden photocurable hydrogel inks, cell viability should be carefully considered due to UV irradiation during photo-crosslinking. Shorter UV irradiation often leads to reasonably high cell viability even though the mechanical stability of photocurable hydrogels is compromised[21,41]. Indeed, there is a significant trade-off between the mechanical performance and cell viability of cell-laden hydrogel scaffolds due to a cytotoxic crosslinking process. Thus, approaches for improving cell viability through a cell protection strategy through the incorporation of plant-derived polyphenols, such as pyrogallol (PG)[21] or improved crosslinking efficiency with dual-photoinitiators,[41] have been proposed. Particularly, using cell-encapsulated Alg microparticles with or without PG treatment, cell-laden hydrogel scaffolds were successfully prepared with minimal death of embedded cells during the whole biofabrication process regardless of UV irradiation time, in our previous study[21]. Thus, this two-step cell seeding approach can be used for gradient hydrogel systems to maximize cell viability during the long and complicated fabrication process.

As DCPD has been widely used for various biomedical applications, particularly in brushite bone cements composed of β-tricalcium phosphate and monocalcium phosphate monohydrate, we postulated that this material system could be utilized to augment bone tissues or soft/hard tissue interfaces in various forms[40]. We assessed the bioactivity of 3D printed HAc-Alg/CaP scaffolds by measuring the expression levels of four representative osteoblastic genes, Runx2, COL1, OPN, and OCN, using directly seeded MC3T3-E1 pre-osteoblasts[42]. As HAc-Alg did not exhibit good cell attachment performance, we were not able to obtain sufficient pre-osteoblasts for phenotypic assessments using the same setup. To overcome this, we set up a cell culture system as a negative control for this *in vitro* differentiation test using commercial cell culture plates. Two types of cell culture media were used in this assay: Cell maintenance medium (negative) and standard osteogenic medium (positive) containing ascorbic acid and Na-β-glycerophosphate (**Figure 7**). Pre-osteoblasts are known to express high levels of COL1 and RunX2 (key markers of early osteogenic differentiation)[42]. Our results indicated that the expression levels of COL1 and RunX2 remained almost the same regardless of the presence of osteogenic reagents or bioactive components such as CaP (**Figure 7A and B**). In contrast, osteogenic medium induced the upregulation of OPN and OCN expressions in pre-osteoblasts cultured in both HAc-Alg/CaP scaffolds and culture plates (**Figure 7C and D**). Although the pre-osteoblasts cultured in composite hydrogel scaffolds (in the presence of osteogenic reagents) exhibited significantly higher gene expression levels of RUX2 and OCN that those grown using culture plates, we could not conclude whether this composite hydrogel system was sufficiently osteoinductive. We have previously implemented HAc-30 wt% CaP hydrogels within subcutaneous

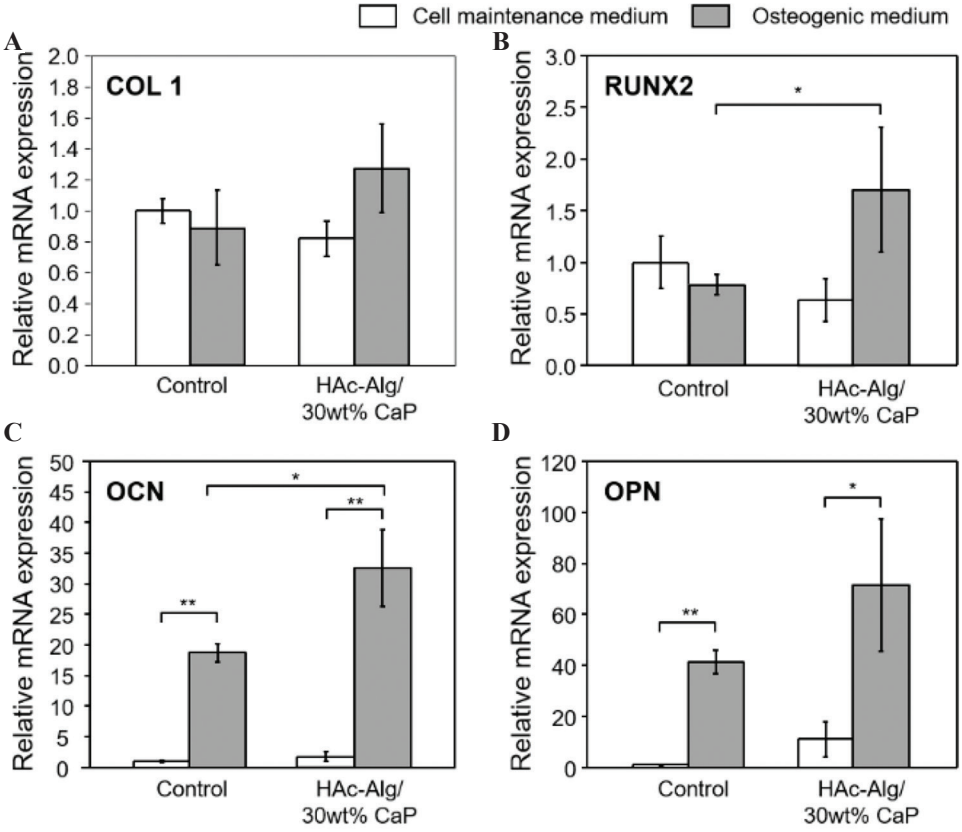

Figure 7. Quantitative gene expression of four markers for *in vitro* cell differentiation. (A) Collagen type 1, (B) RunX2, (C) osteocalcin, and (D) osteopontin of MC3T3-E1 cells after 14 days of culturing on well plate (Control) or three-dimensional printed hyaluronic acid-alginate/30 wt% calcium phosphate composite hydrogel scaffolds with cell maintenance medium or osteogenic medium ($n > 3$, $^{*}P < 0.05$ and $^{**}P < 0.01$).

sites in rats and found no significant mineralization or calcification (despite the strong promotion of soft-tissue regeneration)[5]. Moreover, the cell/matrix interaction is intricate, and numerous factors influence cell differentiation. For instance, the elastic modulus of hydrogels (11 – 30 kPa) was found to lead to osteogenic differentiation of primary human mesenchymal stem cells (hMSCs), whereas softer hydrogels with elastic modulus <5 kPa induce adipogenic lineage of hMSCs[43,44]. The elastic modulus of HAc-30 wt% CaP hydrogel scaffolds was ~ 6 kPa, thus might fail to induce osteogenic lineage of pre-osteoblasts due to insufficient matrix stiffness (**Table 2**). Thus, to enhance the osteoconductive and osteoinductive properties of HAc-Alg/CaP scaffolds, incorporation of additional bioactive additives (e.g., osteogenic reagents and bone growth factors) or mechanical reinforcement agents (e.g., increased mineral or Alg contents) to the hydrogel inks may be essential. In fact, DCPD/OCP has been reported to show lower bioactivity than DCPD with bioglass silica or magnesium[45]. Our follow-up research will expand the applicability of this system with extensive *in vitro* and *in vivo* assessments.

3.6 3D freeform printing for multiphase composite scaffolds

Multi-material 3D printing with nanocomposite hydrogels is challenging because the nanoparticle additives may change the rheological behavior of the composite hydrogel inks depending on the loading amount of the additives[6]. Furthermore, the uniform distribution of nanoparticles requires considerable care when the composite inks are prepared.

Finally, different swelling ratios of nanocomposite hydrogels containing various inorganic contents may lead to the deformation of the multi-material system in water[5]. To show that our method could overcome these problems, *in situ* precipitation of inorganic nanoparticles was carried out directly on

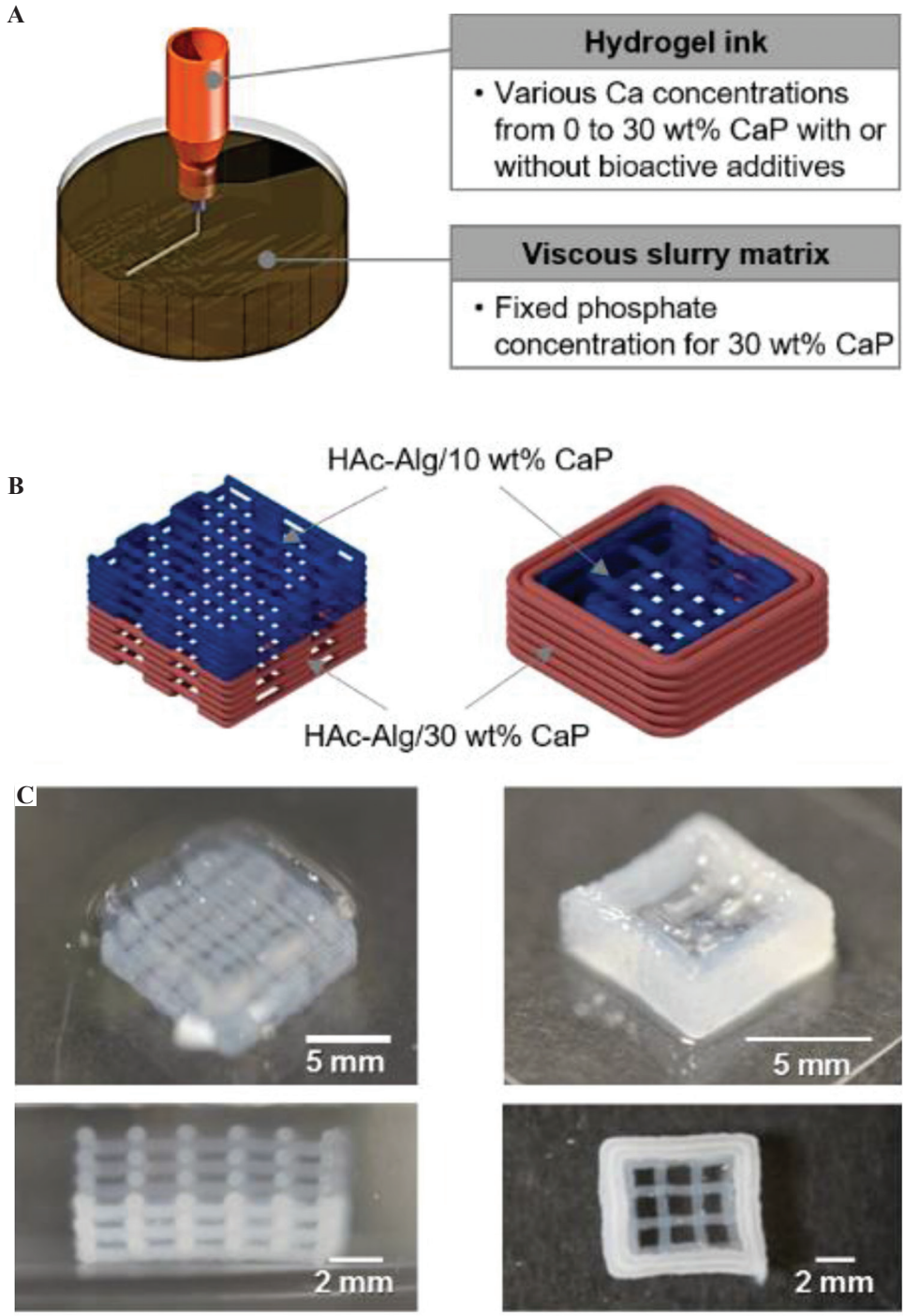

Figure 8. Multiphase material printing with composite hydrogel inks. (A) Three-dimensional (3D) printing strategy of multiphase materials for gradient biomaterials. (B) Schematics of proposed bi-material scaffolds varying mineral contents. (C) Optical images of 3D printed multiphase composite scaffolds composed of hyaluronic acid-alginate (HAc-Alg)/10 wt% calcium phosphate (CaP) and HAc-Alg/30wt% CaP.

a printed hydrogel using their precursors. As proof-of-concept, two multi-material structural designs were created and printed with two nanocomposite hydrogels, HAc-Alg/15 wt% CaP and HAc-Alg/30 wt% CaP (**Figure 8**).

The mineral contents of HAc-Alg/CaP were varied by altering the phosphate ion concentration in the HAc-Alg hydrogel inks, as illustrated in **Figure 8A**. As the precursors of CaP nanoparticles were ions, different concentrations of these precursors did not change the viscosity of the printing inks or gelatin-containing viscous medium. Two types of HAc-Alg inks with different phosphate ion concentrations were printed in a gelatin bath with excess $CaCl_2$ using the same printing parameters. We had already confirmed that the precipitated CaP nanocrystals distributed uniformly within the hydrogel matrix regardless of the precursor concentrations. During 3D printing, the printed inks contained the non-crosslinked GM-HAc liquid phase. Therefore, sequential 3D printing of two different hydrogel inks using only one printer head was feasible. This avoided any interfacial problem because the GM-HAc liquid diffused into the contact region around the joints of the printed filaments, which promoted joint fusion and improved bonding strength among the filaments of the adjacent layers. The two structural designs, vertical stacking and horizontal stacking of the two composite hydrogels resulted in different printing sequence and interfaces between the two materials with different mineral contents (**Figure 8B and C**). In the case of vertical stacking, the bottom layer of HAc-Alg/10 wt% CaP could be deposited on the top layer of HAc-Alg/30 wt% CaP, thus minimizing the time lapse between the printing of each material due to ink change. In contrast, horizontal stacking was achieved by printing the inner part with HAc-Alg/10 wt% CaP, followed by printing the external part of the structure with HAc-Alg/30 wt% CaP (**Supplementary Figure 11**). In this case, the time lapse between the first layers of the two materials was more than 5 min, which was equivalent to the summation of; printing time of the first material and ink change time. However, both printed structures exhibited good mechanical stability and no delamination at the interface of the two materials. More importantly, in the freeform printing of hydrogel inks in aqueous solutions, all of the printed gels were maintained in the swollen state and reacted *in situ* during printing. Thus, the introduction of different materials with various swelling behaviors did not induce any structural mismatch or distortion of the multi-material systems when the hydrogels were immersed in water.

The composite hydrogel systems can be applied for scaffolds of interface tissue engineering (ITE), which aims to regenerate the native enthesis or interface tissue between hard and soft tissues. Thus, ITE requires multiphase and gradient biomaterials to engineer both types of tissue[46-51]. As gradient biomaterials often mimic the complex structures and material properties of each soft and hard tissue, advanced micro- and nano-technologies such as microfluidics, electrospinning, and bioprinting have been introduced into the conventional fabrication process of biomaterials to capture these dimensions[47]. In particular, recent advances in 3D printing technologies have facilitated the development of composite biomaterials through the ability to fabricate structurally, functionally, and compositionally intricate constructs[1-4]. Thus, our approach for multiphase composite scaffolds can be applied for the fabrication of various functional or hybridized gradient biomaterials with complex geometries for ITE scaffolds.

4 Conclusion

In this study, by introducing an *in situ* inorganic nanoparticle precipitation process to a 3D freeform printing system with a two-step crosslinking strategy, we successfully fabricated HAc-Alg/CaP nanocomposite hydrogel scaffolds with various mineral contents and good structural integrity. The first ionic crosslinking of Alg provided structural stability during printing, while the secondary crosslinking of photo-curable GM-HAc improved the mechanical stability of the nanocomposite hydrogels by virtue of the superior bonding

strength of the adjacent layers with well-fused filament joints. The precipitated nanoparticles composed of DCPD and OCP, along with a small amount of calcium carbonate, were uniformly distributed throughout the entire printed hydrogel. The incorporated CaP nanocrystals significantly enhanced the mechanical, physiological, and biological characteristics of the pure hydrogel, suggesting its great potential as a biomaterial for various biomedical applications. In particular, the proposed printing approach allowed multi-phase gradient material printing with a single nozzle system, avoiding any issues caused by the introduction of materials with differences in printability and mechanical stability. Taken together, our results suggest that designing and modifying the printing materials coupled with *in situ* post-printing functionalization and hybridization in reactive viscoplastic matrices, our approach can accelerate the 3D printing of various functional or hybridized gradient biomaterials with complex geometries.

Conflicts of interest and funding

No conflicts of interest were reported by all authors. This research was supported by Nanyang Technological University Start up grant, and A*STAR Advanced Manufacturing and Engineering Individual Research Grants grant A1983c0031 from A*STAR.

Author contributions

Chen S. designed and performed the experiments, data analysis, and drafted the manuscript. Jang T.S. and Jung H.D. conducted SEM/TEM imaging, XRD and EDS analyses of hydrogel samples. Chen S., Pan, M, and Sia M.W performed cell tests. Chong M. and Wang D. designed and supervised the *in vitro* cell experiments. Song J designed the experiments and supervised the whole research. All authors have read the manuscript and given approval to the final version.

References

1. Liu W, Zhang YS, Heinrich MA, *et al*., 2017, Rapid Continuous Multimaterial Extrusion Bioprinting. *Adv Mater*, 29:1604630.
2. Kowsari K, Akbari S, Wang D, *et al*., 2018, High-efficiency High-resolution Multimaterial Fabrication for Digital Light Processing-based Three-dimensional Printing. *3D Print Addit Manuf*, 5:185–93. DOI: 10.1089/3dp.2018.0004.
3. Lopes LR, Silva AF, Carneiro OS, 2018, Multi-material 3D Printing: The Relevance of Materials Affinity on the Boundary Interface Performance. *Addit Manuf*, 23:45–52. DOI: 10.1016/j.addma.2018.06.027.
4. Jang TS, Jung HD, Pan HM, *et al*., 2018, 3D Printing of Hydrogel Composite Systems: Recent Advances in Technology for Tissue Engineering. *Int J Bioprinting*, 4:126.
5. Jeong SH, Koh YH, Kim SW, *et al*., 2016, Strong and Biostable Hyaluronic Acid-calcium Phosphate Nanocomposite Hydrogel via *In Situ* Precipitation Process. *Biomacromolecules*, 17:841–51. DOI: 10.1021/acs.biomac.5b01557.
6. Wust S, Godla ME, Muller R, *et al*., 2014, Tunable Hydrogel Composite with Two-step Processing in Combination with Innovative Hardware Upgrade for Cell-based Three-dimensional Bioprinting. *Acta Biomater*, 10:630–40. DOI: 10.1016/j.actbio.2013.10.016.
7. Thoniyot P, Tan MJ, Karim AA, *et al*., 2015, Nanoparticle-hydrogel Composites: Concept, Design, and Applications of These Promising, Multi-functional Materials. *Adv Sci* (*Weinh*), 2:1400010. DOI: 10.1002/advs.201400010.
8. Gaharwar AK, Schexnailder PJ, Dundigalla A, *et al*., 2011, Highly Extensible Bio-nanocomposite Fibers. *Macromol Rapid Commun*, 32:50–7. DOI: 10.1002/marc.201000556.
9. Leach JB, Bivens KA, Patrick CW, *et al*., 2003, Photocrosslinked Hyaluronic Acid Hydrogels: Natural, Biodegradable Tissue Engineering Scaffolds. *Biotechnol Bioeng*, 82:578–89. DOI: 10.1002/bit.10605.
10. Xu X, Jha AK, Harrington DA, *et al*., 2012, Hyaluronic Acid-based Hydrogels: From a Natural Polysaccharide to Complex Networks. *Soft Matter*, 8:3280–94. DOI: 10.1039/c2sm06463d.
11. Kisiel M, Martino MM, Ventura M, *et al*., 2013, Improving the Osteogenic Potential of BMP-2 with Hyaluronic Acid Hydrogel Modified with Integrin-specific Fibronectin Fragment. *Biomaterials*, 34:704–12. DOI: 10.1016/j.biomaterials.2012.10.015.
12. Li QH, Li M, Zhu PZ, *et al*., 2012, *In Vitro* Synthesis of Bioactive Hydroxyapatite Using Sodium Hyaluronate as a Template. *J Mater Chem*, 22:20257–65. DOI: 10.1039/c2jm33624c.
13. Egorov AA, Fedotov AY, Mironov AV, *et al*., 2016, 3D

Printing of Mineral-polymer Bone Substitutes Based on Sodium Alginate and Calcium Phosphate. *Beilstein J Nanotechnol*, 7:1794–9. DOI: 10.3762/bjnano.7.172.

14. Lee H, Kim Y, Kim S, *et al.*, 2014, Mineralized Biomimetic Collagen/Alginate/Silica Composite Scaffolds Fabricated by a Low-temperature Bio-plotting Process for Hard Tissue Regeneration: Fabrication, Characterisation and *In Vitro* Cellular Activities. *J Mater Chem B*, 2:5785. DOI: 10.1039/c4tb00931b.
15. Bhattacharjee T, Zehnder SM, Rowe KG, *et al*., 2015, Writing in the Granular Gel Medium. *Sci Adv*, 1:e1500655. DOI: 10.1126/sciadv.1500655.
16. Highley CB, Rodell CB, Burdick JA, 2015, Direct 3D Printing of Shear-thinning Hydrogels into Self-healing Hydrogels. *Adv Mater*, 27:5075–9. DOI: 10.1002/adma.201501234.
17. Hinton TJ, Jallerat Q, Palchesko RN, *et al*., 2015, Three-dimensional Printing of Complex Biological Structures by Freeform Reversible Embedding of Suspended Hydrogels. *Sci Adv*, 1:e1500758. DOI: 10.1002/adma.201501234.
18. Hinton TJ, Hudson A, Pusch K, *et al*., 2016, 3D Printing PDMS Elastomer in a Hydrophilic Support Bath via Freeform Reversible Embedding. *ACS Biomater Sci Eng*, 2:1781–6. DOI: 10.1021/acsbiomaterials.6b00170.
19. Rodriguez MJ, Dixon TA, Cohen E, *et al*., 2018, 3D Freeform Printing of Silk Fibroin. *Acta Biomater*, 71:379–87. DOI: 10.1016/j.actbio.2018.02.035.
20. Grosskopf AK, Truby RL, Kim H, *et al*., 2018, Viscoplastic Matrix Materials for Embedded 3D Printing. *ACS Appl Mater Interfaces*, 10:23353–61. DOI: 10.1021/acsami.7b19818.
21. Pan HM, Chen S, Jang TS, *et al*., 2019, Plant Seed-inspired Cell Protection, Dormancy, and Growth for Large-scale Biofabrication. *Biofabrication*, 11:025008. DOI: 10.1088/1758-5090/ab03ed.
22. Furuichi K, Oaki Y, Imai H, 2006, Preparation of Nanotextured and Nanofibrous Hydroxyapatite Through Dicalcium Phosphate with Gelatin. *Chem Mater*, 18:229–34. DOI: 10.1021/cm052213z.
23. Thanh NT, Maclean N, Mahiddine S, 2014, Mechanisms of Nucleation and Growth of Nanoparticles in Solution. *Chem Rev*, 114:7610–30. DOI: 10.1021/cr400544s.
24. Bastami A, Allahgholi M, Pourafshary P, 2014, Experimental and Modelling Study of the Solubility of CO2 in Various CaCl2 Solutions at Different Temperatures and Pressures. *Pet Sci*, 11:569–77. DOI: 10.1007/s12182-014-0373-1.
25. Hosoda N, Kato T, 2001, Thin-film Formation of Calcium Carbonate Crystals: Effects of Functional Groups of Matrix Polymers. *Chem Mater*, 13:688–93. DOI: 10.1021/cm000817r.
26. Gallagher PK, Johnson DW, 1973, The Effects of Sample Size and Heating Rate on the Kinetics of the Thermal Decomposition of CaCO3. *Thermochim Acta*, 6:67–83. DOI: 10.1016/0040-6031(73)80007-3.
27. Li ZY, Su YL, Xie BQ, *et al*., 2013, A Tough Hydrogel-hydroxyapatite Bone-like Composite Fabricated *In Situ* by the Electrophoresis Approach. *J Mater Chem B*, 1:1755–64. DOI: 10.1039/c3tb00246b.
28. Sarvestani AS, He XZ, Jabbari E, 2008, The role of filler-matrix interaction on viscoelastic response of biomimetic nanocomposite hydrogels. *J Nanomater*, 2008:9. DOI: 10.1155/2008/126803.
29. Song X, Zhu C, Fan D, *et al*., 2017, A Novel Human-like Collagen Hydrogel Scaffold with Porous Structure and Sponge-like Properties. *Polymers*, 9:638. DOI: 10.3390/polym9120638.
30. Sarvestani AS, Jabbari E, 2008, A Model for the Viscoelastic Behavior of Nanofilled Hydrogel Composites Under Oscillatory Shear Loading. *Polym Compos*, 29:326–36. DOI: 10.1002/pc.20416.
31. Desimone MF, Helary C, Quignard S, *et al*., 2011, *In Vitro* Studies and Preliminary *In Vivo* Evaluation of Silicified Concentrated Collagen Hydrogels. *ACS Appl Mater Interfaces*, 3:3831–8. DOI: 10.1021/am2009844.
32. van Hoogmoed CG, Busscher HJ, de Vos P, 2003, Fourier Transform Infrared Spectroscopy Studies of Alginate-PLL Capsules with Varying Compositions. *J Biomed Mater Res Part A*, 67A:172–8. DOI: 10.1002/jbm.a.10086.
33. Ibrahim S, Kothapalli CR, Kang QK, *et al*., 2011, Characterization of Glycidyl Methacrylate-crosslinked Hyaluronan Hydrogel Scaffolds Incorporating Elastogenic Hyaluronan Oligomers. *Acta Biomater*, 7:653–65. DOI: 10.1016/j.actbio.2010.08.006.
34. Berzina-Cimdina L, Borodajenko N, 2012, Research of Calcium Phosphates Using Fourier Transform Infrared Spectroscopy. InTech, Rijeka. DOI: 10.5772/36942.
35. Dotzauer DM, Dai J, Sun L, *et al*., 2006, Catalytic Membranes Prepared Using Layer-by-layer Adsorption of Polyelectrolyte/Metal Nanoparticle Films in Porous Supports. *Nano Lett*, 6:2268–72. DOI: 10.1021/nl061700q.
36. Ahmed SR, Kim J, Tran VT, *et al*., 2017, *In Situ* Self-assembly of Gold Nanoparticles on Hydrophilic and Hydrophobic Substrates for Influenza Virus-sensing Platform. *Sci Rep*, 7:44495. Available from: https://www.nature.com/articles/srep44495#supplementary-information. DOI: 10.1038/srep44495.
37. Jakus AE, Taylor SL, Geisendorfer NR, *et al*., 2015, Metallic

Architectures from 3D-printed Powder-based Liquid Inks. *Adv Funct Mater*, 25:6985–95. DOI: 10.1002/adfm.201503921.

38. Murphy WL, Mooney DJ, 2002, Bioinspired Growth of Crystalline Carbonate Apatite on Biodegradable Polymer Substrata. *J Am Chem Soc*, 124:1910−7. DOI: 10.1021/ja012433n.
39. Discher DE, Janmey P, Wang YL, 2005, Tissue Cells Feel and Respond to the Stiffness of Their Substrate. *Science*, 310:1139−43. DOI: 10.1126/science.1116995.
40. Tamimi F, Sheikh Z, Barralet J, 2012, Dicalcium Phosphate Cements: Brushite and Monetite. *Acta Biomater*, 8:474–87. DOI: 10.1016/j.actbio.2011.08.005.
41. Han WT, Jang T, Chen S, *et al*., 2020, Improved Cell Viability for Large-scale Biofabrication with Photo-crosslinkable Hydrogel Systems Through a Dual-photoinitiator Approach. *Biomater Sci*, 8:450–61. DOI: 10.1039/c9bm01347d.
42. Huang W, Yang S, Shao J, *et al*., 2007, Signaling and Transcriptional Regulation in Osteoblast Commitment and Differentiation. *Front Biosci J Virtual Lib*, 12:3068–92. Doi: 10.2741/2296.
43. Huebsch N, Arany PR, Mao AS, *et al*., 2010, Harnessing Traction-mediated Manipulation of the Cell/Matrix Interface to Control Stem-cell fate. *Nat Mater*, 9:518–26. DOI: 10.1038/nmat2732.
44. Bai X, Gao M, Syed S, *et al*., 2018, Bioactive Hydrogels for Bone Regeneration. *Bioact Mater*, 3:401–17.
45. Gaharwar AK, Mihaila SM, Swami A, *et al*., 2013, Bioactive Silicate Nanoplatelets for Osteogenic Differentiation of Human Mesenchymal Stem Cells. *Adv Mater*, 25:3329–36. DOI: 10.1002/adma.201300584.
46. Sahoo S, Teh TK, He P, *et al*., 2011, Interface Tissue Engineering: Next Phase in Musculoskeletal Tissue Repair. *Ann Acad Med Singapore*, 40:245–51.
47. Seidi A, Ramalingam M, Elloumi-Hannachi I, *et al*., 2011, Gradient Biomaterials for Soft-to-hard Interface Tissue Engineering. *Acta Biomater*, 7:1441–51. DOI: 10.1016/j.actbio.2011.01.011.
48. Khanarian NT, Jiang J, Wan LQ, *et al*., 2012, A Hydrogel-mineral Composite Scaffold for Osteochondral Interface Tissue Engineering. *Tissue Eng Part A*, 18:533–45. DOI: 10.1089/ten.tea.2011.0279.
49. Liverani L, Boccaccini AR, 2018, Multilayered Scaffolds for Interface Tissue Engineering Applications. Woodhead Publishing, Sawston, United Kingdom. pp. 107–22.
50. Patel S, Caldwell JM, Doty SB, *et al*., 2018, Integrating Soft and Hard Tissues Via Interface Tissue Engineering. *J Orthop Res*, 36:1069–77. DOI: 10.1002/jor.23810.
51. Bracaglia LG, Smith BT, Watson E, *et al*., 2017, 3D Printing for the Design and Fabrication of Polymer-based Gradient Scaffolds. *Acta Biomater*, 56:3-13. DOI: 10.1016/j.actbio.2017.03.030.